Journal of Biomolecular NMR, 2 (1992) 447–465
ESCOM

J-Bio NMR 080

NMR spectroscopy of hydroxyl protons in aqueous solutions of peptides and proteins

Edvards Liepinsh, Gottfried Otting and Kurt Wüthrich

Institut für Molekularbiologie und Biophysik, Eidgenössische Technische Hochschule-Hönggerberg, CH-8093 Zürich, Switzerland

Received 15 June 1992
Accepted 3 July 1992

Keywords: Protein structure; NMR solution structures; Hydroxyl protons; Protein surface; Proton exchange

SUMMARY

Hydroxyl groups of serine and threonine, and to some extent also tyrosine are usually located on or near the surface of proteins. NMR observations of the hydroxyl protons is therefore of interest to support investigations of the protein surface in solution, and knowledge of the hydroxyl NMR lines is indispensable as a reference for studies of protein hydration in solution. In this paper, solvent suppression schemes recently developed for observation of hydration water resonances were used to observe hydroxyl protons of serine, threonine and tyrosine in aqueous solutions of small model peptides and the protein basic pancreatic trypsin inhibitor (BPTI). The chemical shifts of the hydroxyl protons of serine and threonine were found to be between 5.4 and 6.2 ppm, with random-coil shifts at 4°C of 5.92 ppm and 5.88 ppm, respectively, and those of tyrosine between 9.6 and 10.1 ppm, with a random-coil shift of 9.78 ppm. Since these spectral regions are virtually free of other polypeptide ^{1}H NMR signals, cross peaks with the hydroxyl protons are usually well separated even in homonuclear two-dimensional ^{1}H NMR spectra. To illustrate the practical use of hydroxyl proton NMR in polypeptides, the conformations of the side-chain hydroxyl groups in BPTI were characterized by measurements of nuclear Overhauser effects and scalar coupling constants involving the hydroxyl protons. In addition, hydroxyl proton exchange rates were measured as a function of pH, where simple first-order rate processes were observed for both acid- and base-catalysed exchange of all but one of the hydroxyl-bearing residues in BPTI. For the conformations of the individual Ser, Thr and Tyr side chains characterized in the solution structure with the use of hydroxyl proton NMR, both exact coincidence and significant differences relative to the corresponding BPTI crystal structure data were observed.

INTRODUCTION

The determination of protein structures by NMR is based on the collection of the maximum

* To whom correspondence should be addressed.

Abbreviations and symbols: FID, free induction decay; NOE, nuclear Overhauser effect; 2D, two-dimensional; NOESY, two-dimensional NOE spectroscopy; TOCSY, two-dimensional total correlation spectroscopy; BPTI, basic pancreatic trypsin inhibitor; 5PTI, Brookhaven data bank code for the BPTI crystal structure of Wlodawer et al. (1984); Ac-, acetyl; TFA-, trifluoroacetyl; -OMe, oxymethyl; RMSD, root-mean-square deviation.

0925-2738/$ 5.00

possible number of NOE distance constraints between distinct pairs of protons of the polypeptide chain (Wüthrich, 1986). Therefore, the quality of the structure depends crucially on one's ability to observe and resolve a large number of proton NMR signals. So far, little or no use has been made of the hydroxyl proton resonances of serine, threonine and tyrosine because the intrinsic exchange rates of these hydroxyl protons with water are at least two orders of magnitude faster than those of the backbone amide protons, which are readily observed in H_2O solutions at room temperature and pH values below 7.0 (Wüthrich, 1986). As a consequence, with the experimental conditions commonly used for NMR studies of protein structures, most hydroxyl protons are in the fast-exchange regime where the resonances coalesce with the water signal and all NOEs with the hydroxyl resonances are detected at the water chemical shift (Otting and Wüthrich, 1989; Otting et al., 1991a). Separate observation of the hydroxyl resonances is then of interest both for improved characterization of protein structures and as a reference for studies of protein hydration in solution (Otting et al., 1991b). In the present manuscript we describe experimental conditions for the observation of distinct NMR lines of polypeptide hydroxyl protons in aqueous solutions of peptides and proteins. The practical use of hydroxyl resonances for studies of protein structures is illustrated with a characterization of surface side chains in BPTI.

NMR EXPERIMENTS FOR OBSERVATION OF POLYPEPTIDE HYDROXYL PROTONS

Chemical exchange provides efficient magnetization transfer between hydroxyl protons and water protons, so that separate hydroxyl and water signals can usually be observed only at low temperature. However, even at temperatures near the freezing point of an aqueous solution, commonly used schemes for suppression of the intense water signal by selective irradiation (Wüthrich, 1986) would bleach out the hydroxyl signals due to saturation transfer. Here, we used two spin-lock pulses separated by a free precession period, τ, for water suppression (Otting et al., 1991c). In 2D NMR experiments the use of the spin-lock pulses results in nonuniform spectral excitation in the ω_2-dimension, with a $\sin(\Omega\tau)$ dependence, where Ω is the angular precession frequency relative to the carrier frequency. Thereby zero excitation of the water resonance is achieved by setting the carrier frequency at the frequency of the water line. The use of this solvent suppression technique with NOESY and ROESY experiments has recently been described in detail (Otting et al., 1991c).

In the TOCSY experiment a single spin-lock pulse before acquisition is sufficient to suppress the water resonance, when using MLEV-17 during the mixing time, τ_m, since MLEV-17 has by itself a spin-locking effect (Bax and Davis, 1985; Otting et al., 1991c). The following TOCSY experimental scheme was used:

$$(\pi/2)_{\phi 1} - t_1 - SL_{\phi 2} - \tau_m(\text{MLEV-17}) - \tau - SL_{\phi 3} - \text{acquisition}_{\phi 4} \qquad (1)$$

with the phase cycle $\phi_1 = 2(x,x,-x,-x)$; $\phi_2 = 4(x,-x)$; $\phi_3 = 2(y,-y),2(-y,y)$; $\phi_4 = \phi_1$, where the pulses of the MLEV-17 sequence are cycled together with ϕ_2. Additional incrementation of the phases of all pulses and the receiver in steps of 90° (CYCLOPS) (Hoult and Richards, 1975) results in a 32-step phase cycle. SL denotes spin-lock pulses which are applied with the same power as the other pulses in the scheme. Their duration is typically 0.5 ms and 2.0 ms (Otting et al., 1991c).

The chemical-exchange experiment of Fejzo et al. (1990) was modified to accommodate water suppression by the SL - τ - SL sequence. Loss of magnetization by off-resonance effects was kept to a minimum by including into the mixing period a mixing time with longitudinal relaxation, τ_m^{NOE}, followed by a mixing time with transverse relaxation, τ_m^{ROE}, resulting in the scheme:

$$(\pi/2)_{\phi 1} - t_1 - (\pi/2)_{\phi 2} - \tau_m^{NOE} - (\pi/2)_{\phi 3} - \tau_m^{ROE} - SL_{\phi 4} - \tau - SL_{\phi 3} - \text{acquisition}_{\phi 5} \quad (2)$$

where the ROESY mixing period, τ_m^{ROE}, consists of a train of pulses of 3 μs width, separated by delays of 17 μs (Kessler et al., 1987). τ_m^{NOE} was chosen twice as long as τ_m^{ROE} to properly cancel the NOE cross peaks and select for the chemical-exchange cross peaks. The phase cycle was $\phi_1 = 2(x),2(-x)$; $\phi_2 = 2(x,-x)$; $\phi_3 = 4x$; $\phi_4 = 4y$; $\phi_5 = x,-x,-x,x$, which was extended to 16 steps by CYCLOPS (Hoult and Richards, 1975).

pH-DEPENDENCE OF HYDROXYL PROTON EXCHANGE RATES IN MODEL PEPTIDES

In addition to choosing low temperature and eliminating compounds that might act as catalysts of the exchange (see below), the exchange rates of the hydroxyl protons with water protons can be minimized by the choice of appropriate pH values (Wüthrich, 1986). In practice, knowledge of the pH-dependence of the hydroxyl proton exchange rates is therefore indispensable as a basis for using hydroxyl groups for structural studies. The tetrapeptides TFA-Gly-Gly-Thr-Ala-OMe and TFA-Gly-Gly-Ser-Ala-OMe were used to measure reference hydroxyl proton exchange rates of Thr and Ser representing a 'random coil' peptide environment. For reasons of improved solubility in water, the hydroxyl proton exchange of Tyr was investigated with the compound Ac-Tyr-OMe. Model peptides with protecting groups were selected to prevent catalysis of the hydroxyl proton exchange by backbone carboxyl or amino groups. In all three model compounds the hydroxyl proton resonances could be observed in a mixed solvent of 90% H_2O/10% D_2O at 4°C, with chemical shifts of 5.88 ppm for Thr, 5.92 ppm for Ser and 9.78 ppm for Tyr. The relaxation caused by the chemical exchange with water results in significant line broadening of the hydroxyl proton signals. This exchange broadening was used to determine the rate constants, k_{ex}, of the proton exchange between hydroxyl groups and water according to (see, e.g., Pople et al., 1959)

$$k_{ex} = \pi (\Delta\nu_{obs} - \Delta\nu_{nat}), \quad (3)$$

where $\Delta\nu_{obs}$ is the observed, full line width at half height and $\Delta\nu_{nat}$ is the 'natural' line width, which includes contributions from unresolved scalar couplings and from all relaxation mechanisms other than chemical exchange.

In situations where the exchange contribution to the observed line width is small, the rate constants calculated from Eq. 3 depend critically on the value chosen for the natural line width. Therefore, to obtain a reliable value of $\Delta\nu_{nat}$ we determined the relatively slow exchange rates of the seryl and threonyl hydroxyl protons at pH 6.3, employing a series of three chemical-exchange spectra recorded using the scheme of Eq. 2 with mixing times, $\tau_m^{NOE} + \tau_m^{ROE}$, of 1.4 ms, 2.3 ms and 4.1 ms. From these spectra, the initial build-up rates of the exchange cross-peak volumes were determined, and the volumes of the hydroxyl proton diagonal peaks at zero mixing time were ob-

tained by extrapolation from the diagonal peak volumes measured in the same three spectra. The exchange rate constants were then calculated as the ratio of the initial exchange peak build-up rates over the intensity of the diagonal peaks at zero mixing time (Jeener et al., 1979). The exchange rates at pH 6.3 measured in this way were 44 s^{-1} for Thr and 62 s^{-1} for Ser. This accounts for, respectively, 14 Hz and 19.6 Hz of the total line widths of 21.3 Hz and 29.7 Hz. From Eq. 3 the natural line widths of the hydroxyl proton resonances of Thr and Ser were then determined as 7.3 Hz and 10.1 Hz, respectively. The solubility of the Tyr compound was too low for a determination of the exchange rate from chemical-exchange experiments. Since the Tyr hydroxyl proton has no geminal or vicinal scalar couplings to other protons, its natural line width was taken to be 2.5 Hz, which corresponds to the line width of the acetyl methyl protons in Ac-Tyr-OMe. Using the assumption that the natural line widths are independent of pH and of the proton exchange rate, these values were used as a reference in Eq. 3 to determine the exchange rates at different pH values from the total line widths observed in 1D spectra. Good results were thus obtained in the fast-exchange regime, where the exchange-broadening contributes more than 50 Hz to the total line width, but larger uncertainties result for slow exchange rates, where an error of 1 Hz in the measured exchange-broadening results in a noticeable relative error in k_{ex}.

Logarithmic plots of the exchange rate constants in the model peptides vs. pH (Fig. 1) show straight lines with unit slope, indicating simple first-order rate processes for both acid-catalysed and base-catalysed exchange:

$$k_{ex} = -\frac{\mathrm{d[ROH]}}{\mathrm{[ROH]\,dt}} = k_a\,[\mathrm{H^+}] + k_b\,[\mathrm{OH^-}] \tag{4}$$

[ROH] denotes the NMR signal intensity of the hydroxyl proton, and k_a and k_b are the rate constants for acid and base catalysis, respectively. The pH minima of the exchange rates are quite close to those predicted earlier on the basis of literature data on the equilibrium constants pK_a (Wüthrich, 1986). In contrast to these earlier predictions, however, the hydroxyl proton exchange rates at the pH minima at 4 °C are of the same order of magnitude for Tyr as for Thr and Ser (Fig. 1). The observation of hydroxyl proton resonances in aqueous solution depends critically on the absence of exchange catalysis by impurities (Englander and Kallenbach, 1983). In control experiments we observed a significant increase in the exchange rates in the presence of 25 mM

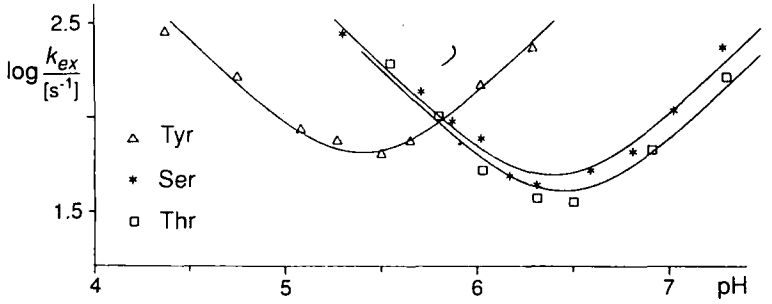

Fig. 1. Logarithmic plots of the exchange rate constants, k_{ex}, at 4°C vs. pH for Thr, Ser and Tyr hydroxyl protons in TFA-Gly-Gly-Thr-Ala-OMe, TFA-Gly-Gly-Ser-Ala-OMe, and Ac-Tyr-OMe, respectively, in a mixed solvent of 90% H_2O/10% D_2O. The experimental points are identified in the figure, the lines represent the best fit of the function described by Eq. 4.

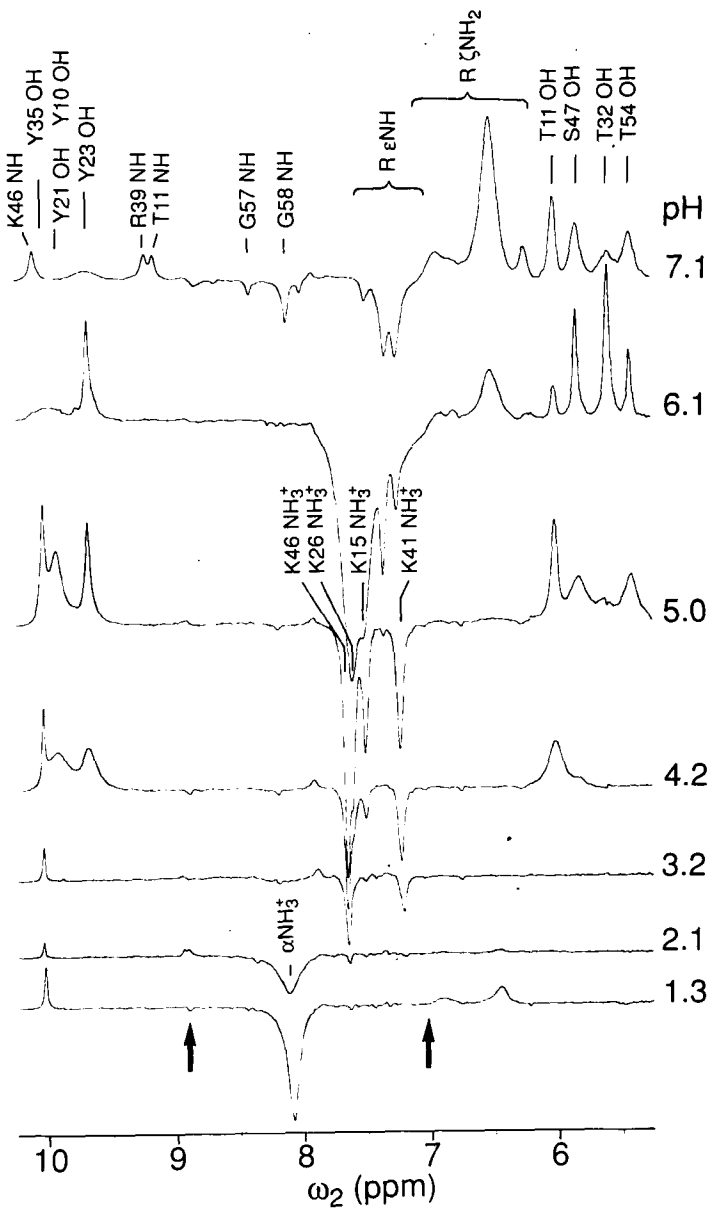

Fig. 2. Cross sections taken along ω_2 at the ω_1 frequency of the water resonance through chemical-exchange spectra of BPTI showing exchange peaks between BPTI protons and water protons at different pH values (BPTI concentration 20 mM, solvent 90% H_2O/10% D_2O, T = 4°C). The spectra were recorded with the scheme of Eq. 2 at 500 MHz on a Bruker AMX 500 spectrometer as 128 × 2048 points time domain matrices using $t_{1max} = 33$ ms, $t_{2max} = 170$ ms, 16 scans/FID, a mixing time, $\tau_m^{NOE} + \tau_m^{ROE}$, of 30 ms and a total experimental time of about 1.4 h per spectrum. The carrier was set at the water frequency and the water signal suppressed by the two spin-lock pulses $SL_{\phi 4} = 0.5$ ms, $SL_{\phi 3} = 2.5$ ms, with $\tau = 510$ μs. The excitation profile along ω_2 is given by $\sin(\Omega\tau)$, where Ω is the angular frequency relative to the carrier frequency. Sign changes in the excitation profile are indicated by the two arrows below the pH 1.3 trace. The spectra were baseline-corrected in both dimensions using polynomials. Selected peaks are labeled with the one-letter amino acid symbol and the sequence position.

phosphate, and the hydroxyl resonances broadened beyond detection in the presence of either 200 mM phosphate or 200 mM acetate even at the pH minima of the exchange rates under salt-free conditions (Fig. 1).

OBSERVATION OF HYDROXYL PROTON NMR LINES IN THE PROTEIN BPTI

Figure 2 shows cross sections along the ω_2-frequency axis at the ω_1 chemical shift of the water resonance through 2D chemical-exchange spectra of BPTI recorded with the scheme of Eq. 2 at 4°C and at different pH values. All cross peaks are due to chemical exchange with water. In particular, the strong NOE cross peaks with the interior hydration water molecules (Otting and Wüthrich, 1989) are not observed in this experiment. The spectral excitation profile was adjusted for optimal detection of the hydroxyl proton resonances of Ser and Thr between 5.4 and 6.2 ppm as well as those of Tyr between 9.6 and 10.1 ppm. Sign changes of the excitation profile occur at 7.0 and 8:9 ppm, which results in negative exchange cross peaks for the resonances of the N-terminal αNH_3^+ group and the lysyl side chains. The chemical exchange with water determines the build-up rate of the cross-peak intensities during the mixing time and provides also the main relaxation mechanism. The strongest cross peaks are therefore observed for intermediate exchange rates, when the exchange with water is faster than the inverse of the mixing time but significantly slower than the chemical-shift difference between the resonances of the labile protons and the water resonance. The exchange cross peaks vanish for both very slow or very rapid exchange. These two limiting situations can be distinguished by the fact that for slowly exchanging protons the diagonal peaks are separated from the water resonance, whereas in the fast-exchange limit the resonances of the exchanging protons are merged with the water line (Otting et al., 1991a).

In Fig. 2 the chemical-exchange spectrum at pH 1.3 contains only the exchange cross peaks from the ζNH_2 groups of arginine side chains around 6.5 ppm, the N-terminal αNH_3^+ group of Arg^1 at 8.2 ppm, and the hydroxyl group of Tyr^{35} at 10.0 ppm. At this pH value the exchange of the seryl and threonyl hydroxyl protons and most of the tyrosyl hydroxyl protons is too rapid to cause observable exchange cross peaks. In contrast, εNH of arginine, the side-chain amino protons of lysine and the backbone amide protons are in the slow-exchange limit at this pH. At pH 2.1 the exchange cross peaks of the Arg ζNH_2 groups vanish due to slowed chemical exchange. At pH 3.2 the peak of the N-terminal αNH_3^+ group disappears due to an increase in the exchange rate with the solvent, and in turn an increase in the exchange rates leads to the appearance of exchange peaks for the side-chain amino protons of the lysyl residues. These disappear again at pH values above 7.0, where the exchange rate becomes very rapid (Wüthrich, 1986). The exchange rates of most of the Tyr hydroxyl protons are slowest near pH 5.0, and those of the hydroxyl protons of serine and threonine near pH 6.0, so that sharp NMR lines can be observed. The assignment of the individual hydroxyl proton resonances was obtained from the intraresidual cross peaks observed in NOESY spectra recorded at these pH values. At pH values above 7.0, increasing exchange rates with water (Wüthrich, 1986) quench the exchange peaks of the hydroxyl protons, while new exchange cross peaks are observed with backbone amide protons and with the εNH and ζNH_2 protons of arginine side chains.

The exchange rates of the hydroxyl protons of Ser and Thr at pH 6.3 were measured from a series of 8 chemical-exchange experiments (Eq. 2) recorded with mixing times in the range 2–16 ms. The ratio of the initial exchange peak build-up rates over the diagonal peak intensities at zero

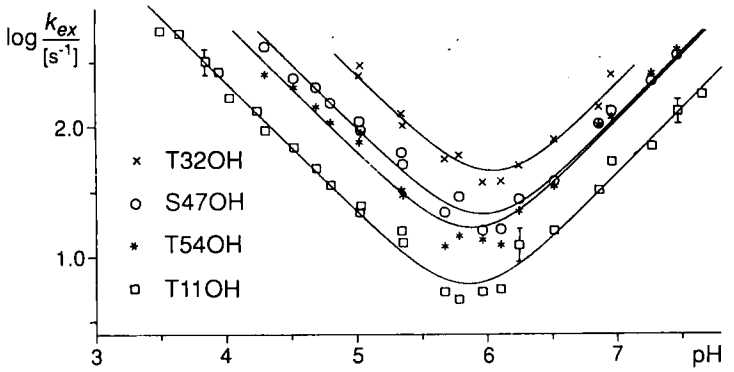

Fig. 3. Logarithmic plots of the exchange rate constants, k_{ex}, at 4°C vs. pH for Thr and Ser hydroxyl protons in BPTI. The experimental points are identified in the figure, the lines show the best fit of Eq. 4. Error bars with three selected data points of Thr[11] indicate the range of rate constants that would be compatible with the measurements. Similar errors are associated with the other OH-exchange curves in this figure and in Fig. 4.

mixing time was determined as described earlier for the model peptides. Combined with the total line widths measured for the OH resonances, the following natural line widths were obtained using Eq. 3: Thr[11], 22.1 Hz; Ser[47], 15.4 Hz; Thr[32], 11.6 Hz; Thr[54], 15.3 Hz. The exchange rates at the other pH values were then determined from the measured total line widths, using these values of $\Delta\nu_{nat}$ in Eq. 3. The logarithmic plots of the rate constants vs. pH (Fig. 3) show straight lines with unit slope, indicating first-order rate processes for both acid- and base-catalysed exchange (Eq. 4) with all Ser and Thr residues.

All OH groups of serine and threonine are solvent exposed both in the NMR solution structure (Berndt et al., 1992) and the X-ray crystal structures of BPTI (Deisenhofer and Steigemann, 1975; Wlodawer et al., 1984,1987). This is now also supported by the pH dependence of the OH exchange rates (Fig. 3), which coincides with that in the well-solvated model peptides by both the unit slope in the acidic and basic pH range and the pH minimum of the exchange rate near pH 6.0.

Three of the four Tyr OH resonances in BPTI show the narrowest lines near pH 5.0 (Fig. 2), which coincides with the data from model peptides (Fig. 1). Tyr[35], however, has the narrowest line width near pH 2.0, where the small size of the exchange peak indicates outstandingly slow exchange with water (Fig. 2). Because of overlap between the OH signals of Tyr[10] and Tyr[21], quantitative exchange rates were determined only for the hydroxyl protons of Tyr[23] and Tyr[35]. To this

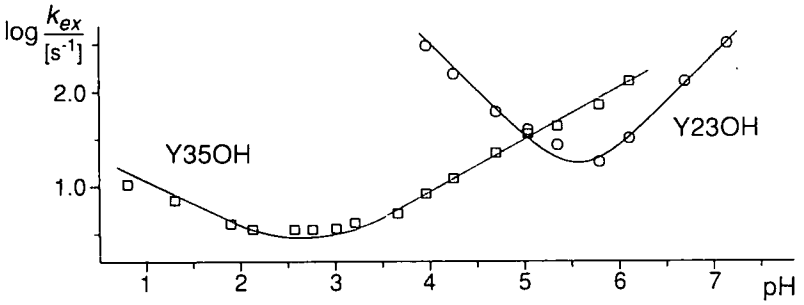

Fig. 4. Logarithmic plots of the exchange rate constants, k_{ex}, at 4°C vs. pH for two Tyr hydroxyl protons in BPTI.

end, the integrals of the exchange cross peaks of the Tyr hydroxyl protons were compared with the integrals of the exchange cross peak of Thr^{11}, for which the exchange rates had previously been measured (Fig. 3). Figure 4 shows that the exchange of the hydroxyl proton of Tyr^{23} can be described by Eq. 4, with equal rates of acid- and base-catalysed exchange near pH 5.6. In contrast, the exchange rate minimum of Tyr^{35} OH is shifted to lower pH and a slope of about 0.5 is observed for both acid- and base-catalysed exchange. Interestingly, in the 3D structure of BPTI the Tyr^{35} hydroxyl proton is more accessible to the solvent than the hydroxyl oxygen atom. Therefore, the protein environment is unfavourable for acid-catalysed exchange of the hydroxyl proton in an S_N2-type reaction by restricting the access of the H_3O^+ ions to the hydroxyl oxygen, but it hinders to a lesser extent the abstraction of the hydroxyl proton by OH^- ions. The steric hindrance of the acid catalysis thus presents an explanation of the fact that the exchange rate minimum is shifted to low pH. The non-unit slopes of the hydroxyl exchange rates vs. pH observed for Tyr^{35} are under continued investigation. Possibly the formation of an intramolecular hydrogen bond of the Tyr^{35} hydroxyl proton with the carbonyl oxygen of Gly^{37} could be the cause of this phenomenon (see below).

CONFORMATION OF THE SER, THR AND TYR SIDE CHAINS OF BPTI IN SOLUTION

The observation of separate, resolved hydroxyl proton resonances enables a more precise determination of the conformation of hydroxyl-bearing side chains, including observations on the spatial orientation of the hydroxyl groups. For Ser and Thr, vicinal scalar coupling constants between the hydroxyl protons and the β-protons, $^3J_{OH\beta}$, were determined from a series of TOCSY spectra recorded with MLEV-17 mixing times, τ_m, of 10, 20, 30 and 40 ms (Eq. 1). The initial build-up rates of the βH-OH cross peaks were determined as the ratio of the cross-peak intensity at 10 ms mixing time over the OH diagonal peak intensity at zero mixing time, where the latter was obtained by extrapolation from the diagonal peak intensities observed at the different mixing

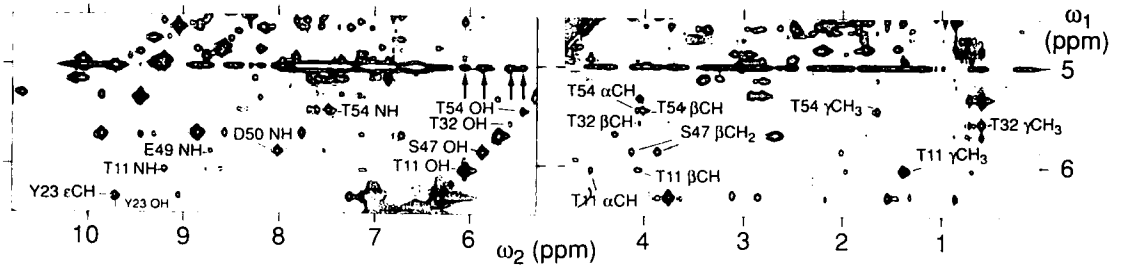

Fig. 5. Spectral regions ($\omega_1 = 4.5$–6.5 ppm, $\omega_2 = 0.0$–4.8 ppm and 5.2–10.8 ppm) of a 600-MHz ^1H NOESY spectrum of BPTI recorded in H_2O at pH 6.3 and 4°C. The experimental scheme of Fig. 1A in Otting et al. (1991c) was used, with a mixing time, τ_m, of 53 ms, spin-lock pulses $SL_{\phi 4} = 0.5$ ms and $SL_{\phi 5} = 2$ ms separated by a delay $\tau = 105$ μs, $t_{1max} = 48$ ms, $t_{2max} = 139$ ms, time domain data size 700 × 2048 data points, 32 scans/FID. To prevent decay of the water signal by radiation damping, homospoil pulses of 0.5 ms duration were applied in 2-ms intervals during the first 20 ms of the mixing time. Peaks identified with the amino acid one-letter symbols and the sequence positions include the diagonal peaks of the hydroxyl protons of Thr^{11}, Thr^{32}, Ser^{47} and Thr^{54}, selected cross peaks with these resonances (identified with the assignment of the coupling partner), and a cross peak with Tyr^{23} OH. The 4 arrows identify the exchange cross peaks of the 4 hydroxyl protons of Ser and Thr with the water line.

times. Comparison of the measured initial build-up rates with the theoretical TOCSY cross-peak build-up rates, $\sin^2(\pi^3 J_{OH\beta}\,\tau_m)$ (Braunschweiler and Ernst, 1983), yielded an estimate for the coupling constants $^3J_{OH\beta}$. For Thr[11], $^3J_{OH\beta}$ was thus found to be larger than 10 Hz, and $^3J_{OH\beta}$ for all other threonyl and seryl residues was smaller than 5 Hz. The large $^3J_{OH\beta}$ coupling in Thr[11] could also be measured from the resolved doublet fine structure of the hydroxyl resonance observed at pH 5.9, yielding $^3J_{OH\beta} = 10.3$ Hz. Overall, these coupling constants indicate that the protons of the H-C$^\beta$-O-H moiety of Thr[11] are in a *trans* conformation, whereas near-*gauche* arrangements are indicated for Thr[32], Ser[47] and Thr[54].

Through observation of NOEs with hydroxyl protons one can locate these protons in the 3D protein structure. Figure 5 shows NOESY cross peaks observed with the hydroxyl protons of Ser and Thr at pH 6.3. For the most rapidly exchanging hydroxyl proton, Thr[32] OH (Fig. 3), the exchange cross peak between the water resonance at $\omega_1 = 5.0$ ppm and the hydroxyl line at $\omega_2 = 5.6$ ppm is more intense than the diagonal peak. This arises because the chemical exchange efficiently relaxes the OH magnetization during the mixing time of 53 ms, whereas the more slowly relaxing water magnetization builds up the exchange peak during the entire mixing period. Table 1 lists the NOESY cross peaks with the hydroxyl protons of BPTI observed at 4°C. Not included are the hydroxyl protons of Tyr[10] and Tyr[21], for which the only observable NOEs were with the ring protons in the ζ-position next to the hydroxyl group.

As all cross peaks with the same OH resonance are similarly affected by the chemical-exchange relaxation of the hydroxyl proton, evaluation of the relative intensities of multiple NOE cross peaks with the same hydroxyl proton resonance will generally constrain the conformation of the hydroxyl groups more stringently than a common calibration curve for all hydroxyl proton resonances (Saulitis and Liepinsh, 1990). Alternatively, absolute cross-peak intensities with the hydroxyl protons can be measured under conditions of relatively slow chemical exchange. In the present investigation we evaluated the NOESY cross-peak intensities with the hydroxyl protons of Thr and Ser at pH 6.3 and those with the hydroxyl protons of Tyr at pH 5.4 (Figs. 3 and 4). In addition, the cross peaks of the most rapidly exchanging hydroxyl proton, Thr[32] OH, were measured with a shorter mixing time (Table 1). Absolute intensities of the hydroxyl proton NOEs were assessed by comparison with the cross peaks between nonlabile protons, and a single calibration curve was used to translate the cross-peak intensities into upper-limit distance constraints (Table 1). These distance constraints were supplemented by dihedral angle constraints derived from the measurements of $^3J_{OH\beta}$. Using these dihedral angle constraints, the hydroxyl proton of Thr[11] was forced into a *trans* orientation with respect to the β-proton by restricting the χ^2-angle to the range $-120° < \chi^2 < 0°$. Similarly, for Thr[32] and Thr[54], where small $^3J_{OH\beta}$ values had been observed, χ^2 was restricted to the range $0° < \chi^2 < 240°$ to exclude the *trans* arrangement of the H-C$^\beta$-O-H moiety. The observation of small $^3J_{OH\beta}$ values for both β-protons of Ser[47] was translated into a χ^2-angle constraint of $60° < \chi^2 < 240°$, which is also indicated by the strong intraresidual βH-OH NOEs.

An extensive NMR data set is available which defines the 3D solution structure of BPTI at 36°C and pH 4.6 to high precision (Berndt et al., 1992). Based on earlier observations that no significant spectral changes occur between 36°C and 4°C, or in the pH range 4.6–6.3 (Wagner, 1977), we determined the solution conformation of the hydroxyl-bearing side chains by supplementing the NMR constraints used previously for the structure calculation at 36°C with the hydroxyl proton constraints measured at 4°C (Table 1) and repeated the complete structure computation using

TABLE I
RELATIVE INTENSITIES OF NOEs WITH HYDROXYL PROTONS IN BPTI, CORRESPONDING UPPER-LIMIT NOE DISTANCE CONSTRAINTS AND PROTON–PROTON DISTANCES IN THE CRYSTAL STRUCTURE 5PTI

NOE assignments[a]	NOE intensity[b]	Constraint (Å)[c]	^{1}H-^{1}H Distance (Å)[d]
$Thr^{11}OH$–$Thr^{11}\gamma CH_3$	135	3.4[e]	2.4
–$Thr^{11}\alpha H$	97	2.6	2.4
–$Thr^{11}\beta H$	67	2.9	3.0
–$Thr^{11}NH$	28	3.6	3.6
–$Tyr^{35}\alpha H$	22	3.8	3.3
–$Val^{34}NH$	14	4.2	3.9
–$Gly^{36}NH$	12	4.4	4.2
–$Val^{34}\gamma^1CH_3$	9	5.6[e]	4.2
–$Phe^{33}\delta^1H$	8	4.9	2.8
–$Val^{34}\beta H$	7	5.0	3.5
–$Phe^{33}\varepsilon^1H$	6	5.3	3.7
–$Val^{34}\gamma^2CH_3$	4	6.6[e]	5.6
$Tyr^{23}OH$–$Ala^{25}\alpha H$	25	3.5	4.5
–$Gly^{28}\alpha^1H$	25	3.5	3.0
–$Gly^{28}\alpha^2H$	18	3.8	4.1
–$Ala^{25}\beta CH_3$	9	5.6[e]	5.9
$Thr^{32}OH$–$Thr^{32}\gamma CH_3$	48	4.1[e]	3.4
–$Thr^{32}\beta H$	48	3.1	2.3
–$Thr^{32}NH$	20	3.8	2.8
$Tyr^{35}OH$–$Tyr^{35}\varepsilon^2H$	100	2.5	2.9
–$Ala^{40}NH$	50	3.0	2.3
–$Ala^{40}\beta CH_3$	50	4.0[e]	2.3
–$Cys^{38}\alpha H$	35	3.3	3.3
–$Arg^{39}NH$	25	3.5	3.6
–$Tyr^{35}\varepsilon^1H$	18	3.8	3.2
–$Gly^{37}\alpha^1H$	12	4.2	4.5
$Ser^{47}OH$–$Ser^{47}\beta^3H$	87	2.6	2.1
–$Asp^{50}NH$	75	2.7	2.6
–$Ser^{47}\beta^2H$	63	2.9	2.6
–$Glu^{49}NH$	19	3.9	3.9
–$Glu^{49}\beta H$	12	5.4[e]	3.1
–$Ser^{47}NH$	5	5.4	3.5
–$Asp^{50}\beta H$	1	8.6[e]	3.2
$Thr^{54}OH$–$Thr^{54}\beta H$	99	2.5	2.2
–$Thr^{54}NH$	75	2.7	2.3
–$Thr^{54}\alpha H$	45	3.1	3.1
–$Phe^{45}\varepsilon^2H$	26	3.6	3.2
–$Thr^{54}\gamma CH_3$	24	4.6[e]	3.5
–$Cys^{55}NH$	11	4.4	4.2
–$Arg^{53}NH$	9	4.7	4.4

the variable target function program DIANA (Güntert et al., 1991a). In an initial round of structure calculations the hydroxyl proton of Thr^{54} was found to be directed towards the Thr^{54} γCH_3 group in 4 of the 20 best structures, in obvious contradiction with the relative NOE intensities of Table 1. Since none of these 4 conformers ranked among the best 10 structures with respect to the residual target function value, the calculations were repeated after addition of a lower-limit constraint of $\geq$ 3.0 Å for the intraresidual distance between the hydroxyl proton and the γCH_3-pseudoatom (Wüthrich, 1986) of Thr^{54}. The residual constraint violations of the final structures obtained with this input were nearly identical to those obtained without hydroxyl proton constraints (Berndt et al., 1992).

Figure 6 affords a comparison between two groups of 20 DIANA conformers representing, respectively, the solution structures of BPTI computed with and without the hydroxyl group constraints. It is seen that the heavy atom positions of all hydroxyl-bearing side chains are well defined by both structure calculations. A visibly improved characterization of the side-chain orientation due to the additional hydroxyl proton constraints is indicated only for Tyr^{23}. However, while the orientations of the hydroxyl groups are basically random in the previously calculated structures (Berndt et al., 1992) (Fig. 6A), all but one are well defined in the structures calculated with hydroxyl-group constraints (Fig. 6B). The exception is Thr^{32}, for which the intraresidual NOEs of Table 1 were insufficient to uniquely define the rotamer position of the hydroxyl group.

The solution structure of BPTI determined without hydroxyl-group constraints (Berndt et al., 1992) is represented by a group of 20 DIANA conformers which had been energy-minimized using a modified version of AMBER (Singh et al., 1986), which includes additional potentials for experimental distance limits (Billeter et al., 1990) and dihedral angle constraints (Widmer et al., 1989). Quite generally, the AMBER force field favours the formation of hydrogen bonds and staggered side-chain conformations, so that it can be expected to influence also the conformations of the side-chain hydroxyl groups. In the present work we used the implementation of the AMBER force field in the energy-minimization program OPAL (Luginbühl, P., Güntert, P., Billeter, M. and Wüthrich, K., unpublished results). Figure 7 displays the energy-minimized structures of the DIANA conformations of Fig. 6 calculated with (Figs. 6B and 7B) and without (Figs. 6A and 7A) NMR constraints for the hydroxyl protons. The comparison between the structures before and after energy minimization shows that the energy force field tends to confine the hydroxyl groups within smaller conformational spaces irrespective of the presence of hydroxyl

---

[a] This column lists the two NOE-related groups of protons.

[b] Measured as cross-peak volumes in NOESY spectra at 4 C with the following experimental parameters: Thr^{11}, Ser^{47} and Thr^{54}, mixing time = 53 ms, pH = 6.3; Thr^{32}, mixing time = 25 ms, pH = 6.3; Tyr^{23} and Tyr^{35}, mixing time = 53 ms, pH = 5.4. The NOE intensities were scaled with respect to cross peaks between nonlabile protons, with the cross peak Tyr^{35} OH-$Tyr^{35}\varepsilon^2$H arbitrarily set equal to 100 as an internal reference.

[c] Upper-limit distance constraints calculated from the NOE intensities using $I/I_0 = d_0^4/d^4$ (Güntert et al., 1991b), where d is the upper-distance limit, I the NOE intensity listed in the second column, and d_0 and I_0 are the corresponding values for the cross peak Tyr^{35} OH-$Tyr^{35}\varepsilon^2$H, for which $d_0 = 2.5$ Å was determined by comparison with NOEs corresponding to known proton–proton distances.

[d] Distance between the two protons listed in the first column in the crystal structure 5PTI (Wlodawer et al., 1984). For methyl and methylene groups only the shortest one of the distances with the individual protons is listed.

[e] Distance referring to a pseudoatom, including a pseudoatom correction of 1.0 Å (Wüthrich, 1986).

B
T11
Y23
T32
A

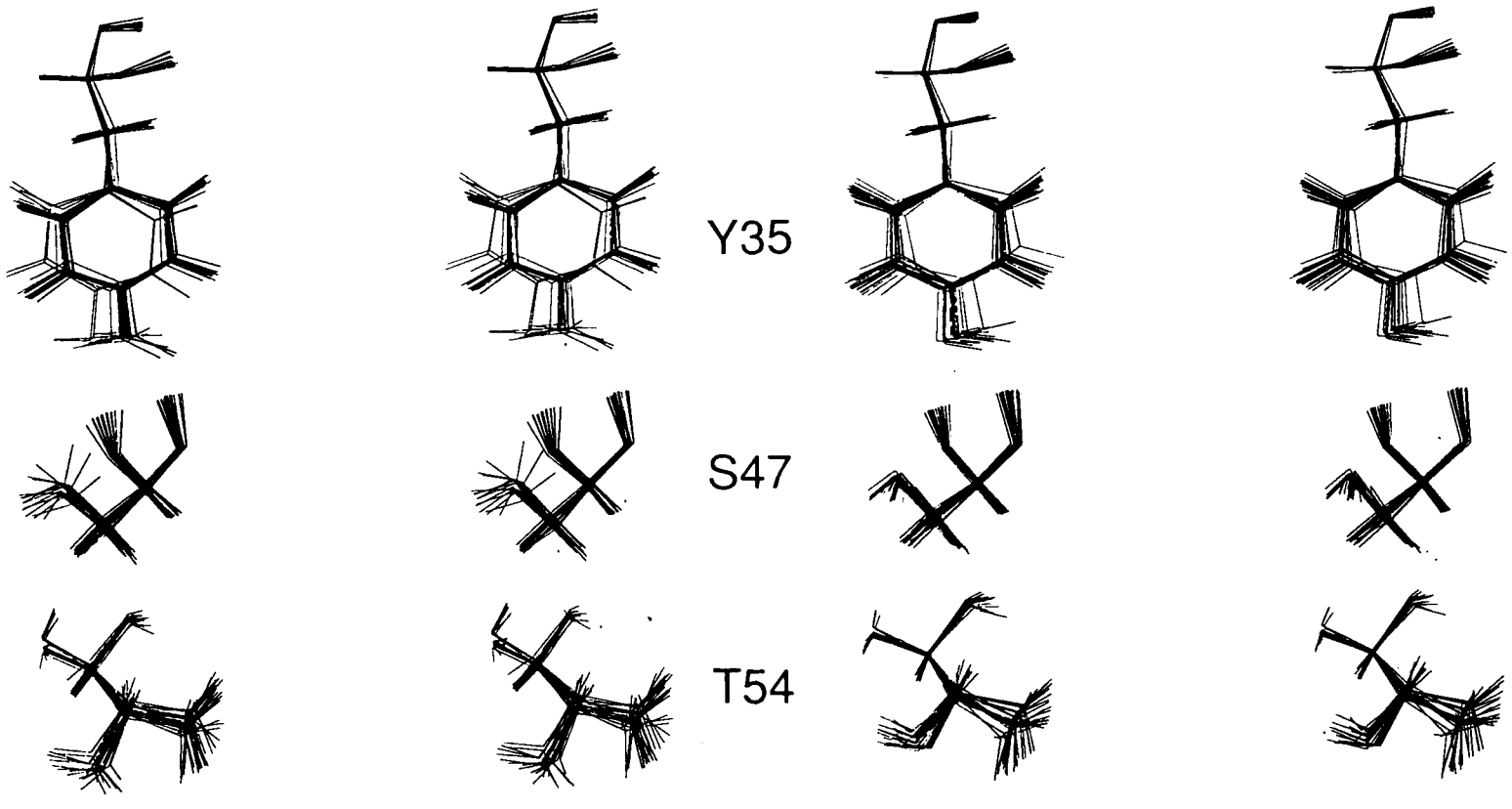

Fig. 6. Stereoviews of the solution structures of the side chains of Thr^{11}, Tyr^{23}, Thr^{32}, Tyr^{35}, Ser^{47} and Thr^{54} in BPTI. To obtain these drawings we superimposed the 20 DIANA conformers for minimal RMSD of the backbone atoms N, C^{α} and C′ in tripeptide segments containing the residue of interest in the central position. All atom representations of the residues are shown, with the amide group to the left or above the carbonyl group. (A) Superposition of the 20 best DIANA structures determined without hydroxyl-group constraints (Berndt et al., 1992). (B) same as (A) but the input for the structure calculations contained the hydroxyl-group constraints.

A
B
T11
Y23
T32

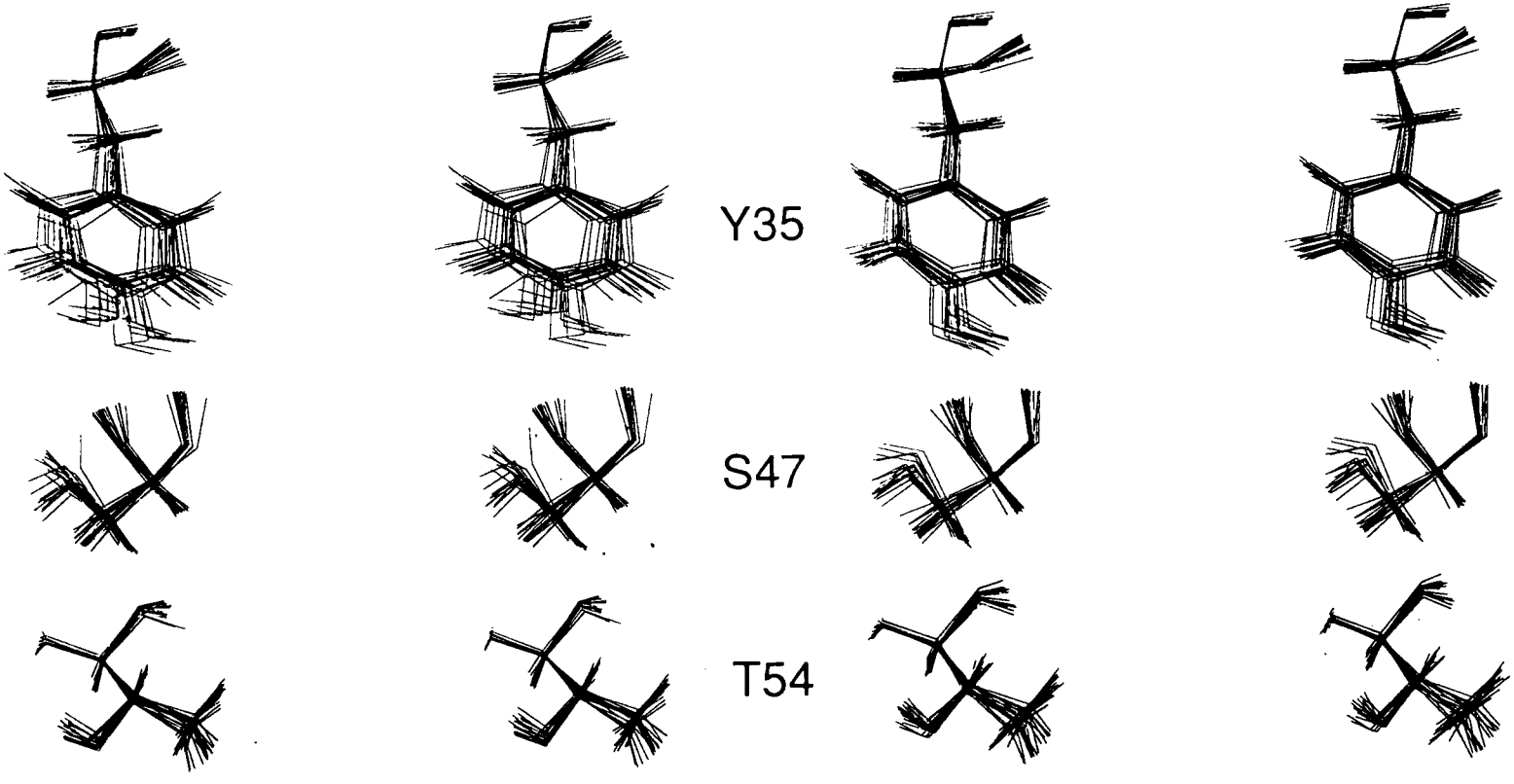

Fig. 7. Stereoview of the solution conformation of the hydroxyl-bearing side chains of BPTI after energy minimization. The same superposition and presentation was used as in Fig. 6. (A) Side-chain conformations calculated without NMR constraints for the hydroxyl groups. (B) Side-chain conformations determined with hydroxyl-group constraints.

proton constraints. Similarly, the methyl groups assume mostly staggered rotamer positions after energy minimization. However, with the exception of Thr^{54}, energy minimization alone was insufficient to uniquely define the hydroxyl group rotamers in the absence of NMR constraints with the hydroxyl protons (compare Figs. 6A and 7A).

After energy minimization of the previous DIANA conformers determined without hydroxyl group constraints (Berndt et al., 1992) the hydroxyl protons of Tyr^{35}, Thr^{11} and Thr^{54} were found to be hydrogen bonded in, respectively, 12, 14 and 20 out of the 20 conformers after energy minimization, using a donor–acceptor distance of less than 2.4 Å together with the requirement of near-linearity as the criterion for hydrogen-bond identification. Thereby the hydrogen bonds Tyr^{35} OH-Cys^{38} C'O and Thr^{11} OH-Val^{34} C'O were also present in, respectively, 7 and 4 conformers before energy minimization, whereas the hydrogen bond Thr^{54} OH-Asp^{50} C'O was formed in all conformers only after the energy minimization. While the presence of the latter two hydrogen bonds was confirmed by the present structure determination, a hydrogen bond Tyr^{35} OH-Cys^{38} C'O is not compatible with the NOE constraints of Table 1, which require that the hydroxyl proton is oriented in the opposite direction. In the present structure determination with hydroxyl group constraints, a hydrogen bond Tyr^{35} OH-Gly^{37} C'O was formed in 3 out of 20 DIANA conformers (Fig. 6B), and in 19 out of 20 conformers after energy minimization (Fig. 7B). The hydroxyl group constraints also promoted the formation of the hydrogen bonds Thr^{11} OH-Val^{34} C'O and Thr^{54} OH-Asp^{50} C'O, which were present in, respectively, 16 and 8 of the 20 DIANA conformers before (Fig. 6B) and in 20 and 19 conformers after energy minimization (Fig. 7B).

COMPARISON OF THE HYDROXYL-BEARING SIDE CHAINS OF BPTI IN SOLUTION AND IN SINGLE CRYSTALS

Three crystal structures of BPTI were solved by X-ray diffraction (Deisenhofer and Steigemann, 1975; Wlodawer et al., 1984, 1987). In all 3 BPTI crystals the heavy atoms superimpose very closely for all hydroxyl-bearing side chains. Since proton coordinates are available from neutron diffraction data of the crystal structure 5PTI only (Wlodawer et al., 1984), we used this structure for the comparison with the solution structure. None of the hydroxyl groups is involved in intermolecular protein–protein contacts in this crystal structure. Figure 8 shows a superposition of the 20 energy-refined DIANA conformers of Fig. 7B with the BPTI crystal structure 5PTI. Close coincidence for the heavy-atom positions is observed between 5PTI and the NMR solution structure (Fig. 8). For the orientation of the O-H bonds, near-coincidence is observed for Thr^{11} and Thr^{54}, whereas conformational differences are indicated for the other hydroxyl-bearing side chains.

More direct evidence for similarities and differences between the NMR solution structure of BPTI and the crystal structures is obtained by comparing the relative intensities of the NOEs involving hydroxyl protons with the corresponding ^1H–^1H distances in the crystal structure (Wlodawer et al., 1984). Table 1 shows that good correlations between the relative NOE intensities measured in solution and the relative distances measured in the crystal structure are observed for the hydroxyl protons of Thr^{11}, Tyr^{35}, Ser^{47} and Thr^{54}. Apparent small discrepancies for some of the NOEs may be explained by spin-diffusion, which tends to falsify the NOE intensities observed for distances longer than about 3.0 Å, and by small conformational differences between the

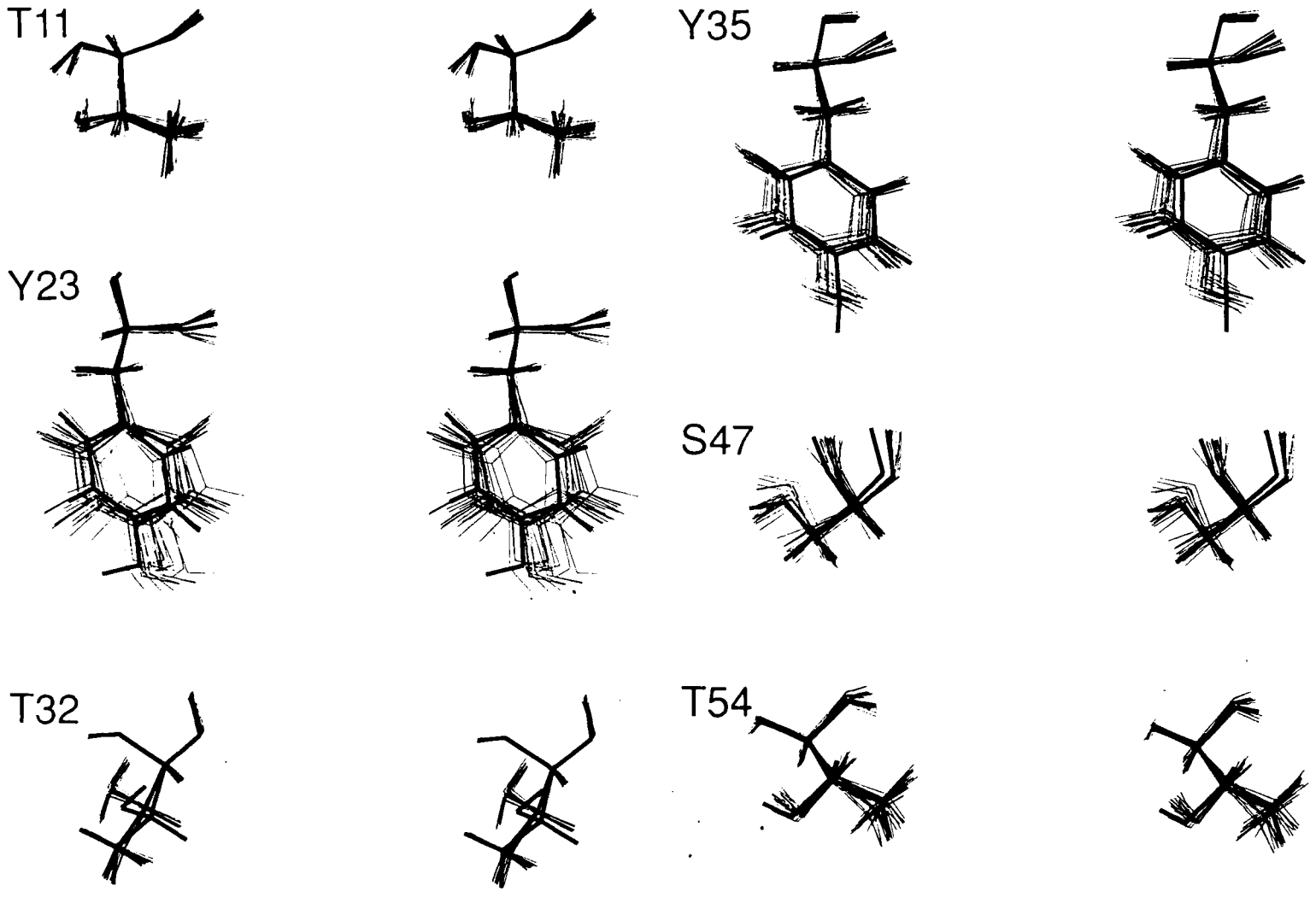

Fig. 8. Stereoview of the superposition of the single-crystal structure 5PTI (Wlodawer et al., 1984) with the energy-refined solution structure of BPTI (Fig. 7B). Same local superposition, representation and orientation as in Figs. 6 and 7. The crystal structure is drawn with a bold line.

solution and the crystal structure. For Thr^{11}, Tyr^{35} and Ser^{47} all proton–proton distances in the crystal structure that are shorter than, respectively, 4.6 Å, 4.3 Å and 3.9 Å gave rise to corresponding observable NOEs in solution. For Thr^{54} a NOE with Arg^{53} β^3H would be expected in addition to those listed in Table 1, since this proton is within 3.0 Å of Thr^{54} OH in the crystal structure. The absence of this NOE is explained by the conformational averaging about the χ^1 angle observed for Arg^{53} in solution (Berndt et al., 1992). Similar to the solution structure (Fig. 7B), the hydroxyl protons of Thr^{54} and Thr^{11} in the crystal structure are hydrogen-bonded to the backbone carbonyl oxygens of Asp^{50} and Val^{34}, respectively. The good agreement of the NOE data and the $^3J_{OH\beta}$ coupling constants with the predictions based on the crystal structure further confirms that these hydrogen bonds are conserved between the crystal and the solution structure. Correspondingly, the hydroxyl proton exchange rates are slower for Thr^{11} and Thr^{54} than for Thr^{32} (Fig. 3), which has no suitable hydrogen-bond acceptor in its vicinity. The hydroxyl proton of Ser^{47} is not hydrogen-bonded in the crystal structure, but is eclipsed with Ser^{47} β^3H (Fig. 8) (Wlodawer et al., 1984). Interestingly, a somewhat larger coupling constant was observed for $^3J_{OH\beta3}$ than for $^3J_{OH\beta2}$, which supports the presence of this eclipsed conformation also in solution. In the crystal structure 5PTI Tyr^{35} is hydrogen bonded to a phosphate molecule. In solution, a much stronger NOE is observed with the ε^2-ring proton than with the ε^1-proton (Table 1). Although the crystal structure of the Tyr^{35} OH group would otherwise be compatible with the relative NOE intensities of Table 1, this appears to support a somewhat different conformation of the side-chain OH group in solution. For Tyr^{23}, inspection of the crystal structure (Fig. 8) shows that good agreement with the NMR data would only be achieved if its OH group were rotated by about 180° around the C-O bond. For Thr^{32} it cannot be decided from the presently available NMR data whether the hydroxyl group assumes the same or different conformations in solution and in the crystals. There is no atom group within suitable distance to form an intraprotein hydrogen bond with this hydroxyl proton, and a dynamic equilibrium between different rotamers may prevail in solution.

CONCLUSIONS

In a qualitative way the NOE signals with a hydroxyl proton can be used as markers for the identification of potential hydrogen-bonding partners of the hydroxyl oxygen atom. For example, in BPTI the NOEs of Ser^{47} OH with the amide protons of Glu^{49} and Asp^{50} (Fig. 5) immediately suggest that the hydroxyl oxygen of Ser^{47} is in a hydrogen bond with the amide proton of Asp^{50} (Berndt et al., 1992), forming an N-cap at the outset of the α-helix (Richardson and Richardson, 1988; Serrano and Fersht, 1989). This is further corroborated by the slowed amide proton exchange rate of Asp^{50} (Wagner and Wüthrich, 1982).

The observation of NOEs with individual hydroxyl proton resonances is particularly important in studies of protein hydration, because NOEs and exchange peaks observed with the separate OH resonances may explain the origin of some of the NOEs observed with different conditions between the water signal and nonlabile protons in close spatial proximity to hydroxyl groups (Otting et al., 1991b,1992).

We foresee that the measurement of NMR constraints with hydroxyl protons of surface side chains will become a routine tool for the improved characterization of protein surfaces in aqueous solution. The information content accessible by the observation of hydroxyl protons has pre-

viously also been recognized in the study of carbohydrates (Harvey et al., 1976; Leroy et al., 1985; Leeflang and Vliegenthart, 1990; Adams and Lerner, 1992; Poppe et al., 1992).

ACKNOWLEDGEMENTS

We thank P. Güntert for the structure calculations of BPTI with inclusion of the hydroxyl group constraints in the input data set, T.H. Xia for the program XAM used to calculate and plot the superpositions in Figs. 6–8, K.D. Berndt for the best-fit program used to plot Figs. 1, 3 and 4, and Mr. R. Marani for the careful processing of the manuscript. Financial support was obtained from the Schweizerischer Nationalfonds (Project 31.32033.91).

REFERENCES

Adams, B. and Lerner, L. (1992) *J. Magn. Reson.*, **96**, 604–607.
Bax, A. and Davis, D.G. (1985) *J. Magn. Reson.*, **65**, 355–360.
Berndt, K.D., Güntert, P., Orbons, L.P.M. and Wüthrich, K. (1992) *J. Mol. Biol.*, in press.
Billeter, M., Schaumann, T., Braun, W. and Wüthrich, K. (1990) *Biopolymers*, **29**, 695–706.
Braunschweiler, L. and Ernst, R.R. (1983) *J. Magn. Reson.*, **53**, 521–528.
Deisenhofer, J. and Steigemann, W. (1975) *Acta Crystallogr. Sect. B*, **31**, 238–250.
Englander, S.W. and Kallenbach, N.R. (1983) *Q. Rev. Biophys.*, **16**, 521–655.
Fejzo, S., Westler, W.M., Macura, S. and Markley, J. (1990) *J. Am. Chem. Soc.*, **112**, 2574–2577.
Güntert, P., Braun, W. and Wüthrich, K. (1991a) *J. Mol. Biol.*, **217**, 517–530.
Güntert, P., Qian, Y.Q., Otting, G., Müller, M., Gehring, W. and Wüthrich, K. (1991b) *J. Mol. Biol.*, **217**, 531–540.
Harvey, J.M., Symons, M.C.R. and Naftalin, R.J. (1976) *Science*, **261**, 435–436.
Hoult, D.I. and Richards, R.E. (1975) *Proc. R. Soc. London, Ser. A*, **344**, 311–340.
Jeener, J., Meier, B.H., Bachmann, P. and Ernst, R.R. (1979) *J. Chem. Phys.*, **71**, 4546–4553.
Kessler, H., Griesinger, C., Kerssebaum, R., Wagner, K. and Ernst, R.R. (1987) *J. Am. Chem. Soc.*, **109**, 607–609.
Leeflang, B.R. and Vliegenthart, J.F.G. (1990) *J. Magn. Reson.*, **89**, 615–619.
Leroy, J.L., Broseta, D. and Guéron, M. (1985) *J. Mol. Biol.*, **184**, 165–178.
Otting, G. and Wüthrich, K. (1989) *J. Am. Chem. Soc.*, **111**, 1871–1875.
Otting, G., Liepinsh, E. and Wüthrich, K. (1991a) *J. Am. Chem. Soc.*, **113**, 4363–4364.
Otting, G., Liepinsh, E. and Wüthrich, K. (1991b) *Science*, **254**, 974–980.
Otting, G., Liepinsh, E. and Wüthrich, K. (1991c) *J. Biomol. NMR*, **1**, 209–215.
Otting, G., Liepinsh, E. and Wüthrich, K. (1992) *J. Am. Chem. Soc.*, in press.
Pople, J.A., Schneider, W.G. and Bernstein, H.J. (1959) *High-resolution Nuclear Magnetic Resonance*, McGraw-Hill, New York, NY, p. 225.
Poppe, L., Stuike-Prill, R., Meyer, B. and van Halbeek, H. (1992) *J. Biomol. NMR*, **2**, 109–136.
Richardson, J.S. and Richardson, D.C. (1988) *Science*, **240**, 1648–1652.
Saulitis, J. and Liepinsh, E. (1990) *J. Magn. Reson.*, **87**, 80–91.
Serrano, L. and Fersht, A.R. (1989) *Nature*, **342**, 296–299.
Singh, U.C., Weiner, P.K., Caldwell, J.W. and Kollmann, P.A. (1986) *AMBER 3.0*, University of California, San Francisco, CA.
Wagner, G. (1977) *Konformation und Dynamik von Proteinase-Inhibitoren: ^{1}H NMR-Studien*, Ph.D. thesis No. 5992, ETH Zürich.
Wagner, G. and Wüthrich, K. (1982) *J. Mol. Biol.*, **160**, 343–369.
Widmer, H., Billeter, M. and Wüthrich, K. (1989) *Proteins*, **6**, 357–371.
Wlodawer, A., Walter, J., Huber, R. and Sjölin, L. (1984) *J. Mol. Biol.*, **180**, 301–329.
Wlodawer, A., Nachman, J., Gilliland, G.L., Gallagher, W. and Woodward, C. (1987) *J. Mol. Biol.*, **198**, 469–480.
Wüthrich, K. (1986) *NMR of Proteins and Nucleic Acids*, Wiley, New York, NY.